www.nature.com/modpathol

ARTICLE

TSC2-mutant uterine sarcomas with *JAZF1-SUZ12* fusions demonstrate hybrid features of endometrial stromal sarcoma and PEComa and are responsive to mTOR inhibition

Sarah Chiang[1]✉, Varshini Vasudevaraja[2], Jonathan Serrano[2], Colin J. R. Stewart[3], Esther Oliva[4], Amir Momeni-Boroujeni[1], Achim A. Jungbluth[1], Arnaud Da Cruz Paula[5], Edaise M. da Silva[1], Britta Weigelt[1], Kay J. Park[1], Robert A. Soslow[1,6], Rajmohan Murali[1], Lora H. Ellenson[1], Ryma Benayed[1], Marc Ladanyi[1], Nadeem R. Abu-Rustum[5,7], Mark A. Dickson[8,9], Seth Cohen[10], Carol Aghajanian[9,10], Martee L. Hensley[9,10], Cheng-Han Lee[11], Matija Snuderl[2] and Jason A. Konner[9,10]✉

Uterine perivascular epithelioid cell tumor (PEComa) is a rare mesenchymal neoplasm that occasionally shares morphologic and immunohistochemical overlap with low- and high-grade endometrial stromal sarcoma (LGESS and HGESS). In this study, we sought to characterize the clinical, morphologic, genetic, and epigenetic features of five uterine sarcomas that display histologic features of LGESS, HGESS, and PEComa. All tumors demonstrated epithelioid cells often associated with a low-grade spindled component resembling LGESS, with both regions expressing CD10, ER, PR, variable HMB45, and Melan-A immunoreactivity, and strong cathepsin K and pS6 expression. Targeted massively parallel sequencing analysis revealed the presence of somatic *TSC2* mutations in all five cases, of which four harbored concurrent or consecutive *JAZF1-SUZ12* gene fusions. Unsupervised hierarchical clustering analysis of methylation profiles of *TSC2*-mutant uterine sarcomas ($n = 4$), LGESS ($n = 10$), and HGESS ($n = 12$) demonstrated two clusters consisting of (1) all LGESS and *TSC2*-mutant uterine sarcomas and (2) all HGESS. KEGG pathway analysis detected methylation differences in genes involved in PI3K/AKT, calcium, and Rap1 signaling. *TSC2*-mutant uterine sarcomas were responsive to hormone suppression, and mTOR inhibition demonstrated clinical benefit in four patients with these neoplasms. Our results suggest that these tumors represent histologically distinctive LGESS with *TSC2* mutations. *TSC2* mutations and *JAZF1-SUZ12* fusion may help diagnose these tumors and possibly direct effective treatment.

Modern Pathology (2022) 35:117–127; https://doi.org/10.1038/s41379-021-00922-7

INTRODUCTION

Perivascular epithelioid cell tumors (PEComas) are rare mesenchymal neoplasms characterized by epithelioid morphology and myomelanocytic differentiation[1,2]. Sporadic and syndromic PEComas, the latter occurring in hereditary tuberous sclerosis complex (TSC), often harbor loss-of-function mutations in *TSC1* or *TSC2*, resulting in activation of the mammalian target of rapamycin (mTOR) pathway[3]. Some PEComas are driven by *TFE3* or *RAD51B* gene rearrangements, the latter found exclusively in uterine tumors[4–6]. Pathology criteria for diagnosing uterine PEComa remain controversial due to significant morphologic and immunohistochemical overlap with uterine smooth muscle neoplasia and lack of established diagnostic criteria[4,7–10]. There is also no consensus regarding management, although mTOR inhibitors (mTORi) appear beneficial when *TSC1/2* mutations are present[11–13].

Uterine PEComa and low- and high-grade endometrial stromal sarcoma (LGESS and HGESS) share morphologic features. Vang and Kempson recognized some uterine PEComas characterized by epithelioid and sometimes spindled cells associated with stromal hyalinization and permeative myoinvasion similar to LGESS[14]. Hornick and Fletcher described similar histologic findings among sclerosing PEComas[15]. However, this morphology appears rare in more recent studies describing uterine PEComas {Bennett, 2018 #806;Schoolmeester, 2014 #810}.

In this study, we sought to characterize the clinical, morphologic, genetic, and epigenetic features of uterine sarcomas that display LGESS, HGESS, and PEComa histologic features and determine whether they represent a distinct uterine sarcoma subtype underpinned by disease-specific genetic alterations. To this end, we performed immunohistochemical characterization,

[1]Department of Pathology, Memorial Sloan Kettering Cancer Center, New York, NY, USA. [2]Department of Pathology, New York University Langone Health and School of Medicine, New York, NY, USA. [3]Department of Histopathology, King Edward Memorial Hospital, Perth, WA, Australia. [4]Department of Pathology, Massachusetts General Hospital and Harvard Medical School, Boston, MA, USA. [5]Department of Surgery, Gynecologic Oncology Service, Memorial Sloan Kettering Cancer Center, New York, NY, USA. [6]Department of Pathology and Laboratory Medicine, Weill Cornell Medical College, New York, NY, USA. [7]Department of Surgery, Weill Cornell Medical College, New York, NY, USA. [8]Department of Medicine, Sarcoma Medical Oncology Service, Memorial Sloan Kettering Cancer Center, New York, NY, USA. [9]Department of Medicine, Weill Cornell Medical College, New York, NY, USA. [10]Department of Medicine, Gynecologic Medical Oncology Service, Memorial Sloan Kettering Cancer Center, New York, NY, USA. [11]Department of Pathology and Laboratory Medicine, BC Cancer and University of British Columbia, Vancouver, BC, Canada. ✉email: chiangs@mskcc.org; konnerj@mskcc.org

Received: 16 April 2021 Revised: 31 August 2021 Accepted: 31 August 2021
Published online: 24 September 2021

targeted DNA- and RNA-based next-generation sequencing (NGS), and methylation profiling of these tumors.

MATERIALS AND METHODS

Case selection

The index case was a recurrent LGESS (Case3-Recur2) found to harbor *TSC2* p.C646* and p.W1194* mutations identified by clinical Memorial Sloan Kettering-Integrated Mutational Profiling of Actionable Cancer Targets (MSK-IMPACT) sequencing. An in-frame fusion between *JAZF1* exon 3 and *SUZ12* exon 2 was detected in an earlier recurrence (Case3-Recur1) of the index case by the MSK-Solid Fusion Assay. A pathology database search for LGESS, HGESS, and PEComa harboring *TSC1/2* mutations in 2003–2021 was conducted and identified four additional cases. Institutional Review Board approval was obtained at Memorial Sloan Kettering Cancer Center (MSKCC). All available pathology slides and reports were reviewed by expert gynecologic pathologists. The number of hematoxylin-and-eosin stained slides reviewed was as follows: 28, 5, and 10 from hysterectomy (Case1-Prim), lung wedge biopsy (Case1-Met1), and vulvar resection (Case1-Recur1) specimens of Case 1, respectively; 1, 1, and 1 from lymph node (Case1-Met1), vaginal (Case2-Met2), and retroperitoneal (Case2-Met3) biopsy specimens of Case 2, respectively; 5, 34, and 18 from endometrial curettage (Case3-Prim), pelvic tumor debulking (Case3-Recur1), and sigmoid resection (Case3-Recur2) specimens of Case 3, respectively; 46, 2, and 1 from hysterectomy (Case4-Prim), pelvic sidewall resection (Case4-Recur1), and bladder soft tissue resection (Case4-Recur2) specimens of Case 4, respectively; 9 and 2 from hysterectomy (Case5-Prim) and lung wedge biopsy (Case5-Met1) specimens of Case 5, respectively. Electronic medical records were reviewed for the date of and stage at diagnosis, treatment, and response to therapy. Overall survival was defined as the time interval from the date of diagnosis to date of death or last follow-up. Patients were seen at MSKCC at initial diagnosis ($n = 3$) or at first recurrence ($n = 2$).

Immunohistochemistry

Immunohistochemistry was performed on 5-µm, formalin-fixed, paraffin-embedded (FFPE) tissue sections using automated staining platforms (Bond III, Leica Biosystems, Buffalo Grove, IL; BenchMark ULTRA, Roche Diagnostics, Indianapolis, IN). Primary antibodies included CD10 (RTU, SP67, Roche), ER (RTU, 6F11, Leica), PR (RTU, 16, Leica), desmin (RTU, DER11, Roche), SMA (1:200, 1A4, Cell Marque), HMB45, A103, cathepsin K, phospho-S6 (pS6; Ser235/236; 1:100, D57.2.2E, Cell Signaling Technology), cyclin D1 (1:100, RM-9104-S, Thermo), and BCOR (1:150, C-10, Santa Cruz) {Lewis, 2018 #821;Chiang, 2017 #822;Schoolmeester, 2015 #823}. Percentage of positive tumor cells was recorded. Intensity of staining was recorded as weak (1), moderate (2), and strong (3). For all immunohistochemical markers, a combined score was calculated as intensity multiplied by percentage of positive cells. BCOR and cyclin D1 were considered positive if the combined score was ≥1.5 and negative if the combined score was <1.5.

Targeted massively parallel sequencing

Tumor samples were subjected to targeted RNA NGS using the MSK-Solid Fusion assay, a custom panel utilizing Archer Anchored Multiplex PCR technology to detect gene fusions and oncogenic isoforms in selected protein-coding exons of 62 genes[16]. Tumor RNA was extracted from macrodissected 5-µm FFPE tissue sections, followed by cDNA synthesis and library preparation. Final targeted amplicons were sequenced on an Illumina Miseq instrument. Data were analyzed using the Archer™ analysis software V5.0.

Tumor and matched peripheral blood samples from five patients were subjected to targeted DNA NGS using MSK-IMPACT ($n = 4$), a hybridization capture-based assay that targets all coding exons and selected regulatory regions and introns of 410 ($n = 1$) or 468 ($n = 3$) key cancer-associated genes[17,18], and Caris Next Generation Profiling ($n = 1$). Tumor DNA was extracted from macrodissected FFPE tissue sections. DNA was sequenced to an average of 677-fold (range, 513- to 1093-fold) sequence coverage. The functional impact of detected non-synonymous somatic mutations was categorized as oncogenic/likely oncogenic, or variants of unknown significance using OncoKB (http://oncokb.org), a precision oncology knowledge base maintained at MSKCC[19]. De-identified patient-level clinical and genomic data are available in cBioPortal.

Fluorescence in situ hybridization

For any case in which targeted RNA NGS failed or did not detect a gene fusion, the FFPE tumor sample was subjected to fluorescence in situ hybridization (FISH) using *JAZF1* break-apart probes (ZytoLight SPEC JAZF1, Zytovision, Bremerhaven, Germany). Slides were deparaffinized, pre-treated, and hybridized with denatured probes overnight, followed by posthybridization washes and counterstaining with DAPI. A Zeiss fluorescence microscope was used to analyze 100 cells (Zeiss Axioplan, Oberkochen, Germany). Gene rearrangement was confirmed if break-apart signals were seen in ≥10% of cells.

Methylation data analysis

Tumor DNA was extracted using automated Maxwell Promega system (Promega, Madison, WI) from available macrodissected FFPE tissue sections of *TSC2*-mutant tumors in the study cohort [$n = 4$ (*JAZF1-SUZ12* fusion, $n = 3$; negative fusion, $n = 1$)] as well as comparison groups consisting of morphologically conventional LGESS [$n = 10$ (*JAZF1-SUZ12* fusion, $n = 2$; *JAZF1-PHF1* fusion, $n = 2$; unknown fusion status, $n = 6$)] and HGESS [$n = 12$ (*YWHAE-NUTM2A/B* fusion, $n = 8$; *ZC3H7B-BCOR* fusion, $n = 4$)] confirmed by expert gynecologic pathologists. Methylation profiling was performed at the New York University Department of Molecular Pathology using the Illumina EPIC 850 Bead-Chip (850K) array to determine the DNA methylation status of >850,000 CpG sites (Illumina, San Diego, CA)[20]. DNA methylation data were analyzed by a Sarcoma Classifier (www.molecularsarcomapathology.org), as recently described[21]. In addition, we performed an unsupervised analysis of the DNA methylation data. Raw methylation data generated from iScan were processed and analyzed with the Bioconductor R package Minfi[22]. All Illumina array probes were normalized using quantile normalization and corrected for background signal. Samples were checked for quality using mean detection p values, and probes with mean detection p value <0.05 were used for further downstream analysis. Beta values were obtained from probes that passed quality control as mentioned above. Heatmaps were generated in an unsupervised manner using hierarchical clustering from ComplexHeatmap R package, with red and blue representing hyper- and hypomethylation, respectively.

Pathway analysis

Kyoto Encyclopedia of Genes and Genomes (KEGG) pathway analysis using R package ClusterProfiler was used to find signaling pathways enriched in the top 10,000 most variable methylation genes/probes[23]. Dot plots represent the ratio of genes (x-axis) involved in each signaling pathway (y-axis) of KEGG database. Size of the dots represents gene counts, and the color denotes significance level.

RESULTS

Clinicopathologic features

We identified five patients with uterine sarcomas harboring *TSC2* mutations; four had concurrent or consecutive *JAZF1-SUZ12* fusion (Tables 1 and 2 and Fig. 1). The median patient age at diagnosis was 55 (range, 46–61) years. Four patients had FIGO stage III or IV disease at diagnosis. Patients were diagnosed with LGESS ($n = 3$, Cases 1–3), HGESS ($n = 1$, Case 4), and malignant PEComa ($n = 1$, Case 5).

Case 1

A 46-year-old patient underwent an urgent total abdominal hysterectomy and bilateral salpingo-oophorectomy (TAHBSO) (Case1-Prim) for vaginal bleeding (Table 1 and Fig. 1). She had lung nodules (Case1-Met1) resected shortly after diagnosis and began megestrol acetate. Residual lung nodules improved based on a CT three months later; however, at that time, she developed a new, hemorrhagic vaginal metastasis and received external beam radiation therapy (EBRT, 4500 cGy) to whole pelvis. She continued megestrol acetate for 11 months, when it was stopped for weight gain and replaced with letrozole. After 1 month, she developed arthralgias and switched to exemestane, which she continued without disease recurrence for 11 years, then stopped. Two years after treatment cessation, she developed radiologic evidence of retroperitoneal and pelvic lymphadenopathy, lung nodules, and a vulvar metastasis (Case1-Recur1), which was resected. Exemestane was resumed; however, she progressed after six months, and then received fulvestrant for eight months before she again progressed.

Table 1. Patient characteristics, initial diagnosis, and outcomes.

Case	Age at diagnosis (y)	Initial diagnosis	FIGO stage at diagnosis	Time from initial resection to recurrence (mo)	Sites of disease at time of marker-directed therapy	Time to last follow-up or death	Status at last follow-up
1	46	LGESS	IVB	N/A	Lymph node, lung, vulva, bone	16 y 11 mo	AWD
2	61	LGESS	IVB	N/A	Lymph node, lung, peritoneum, pelvis	2 y 6 mo	AWD
3	55	LGESS	IA	37	Liver, peritoneum, vagina	9 y 5 mo	AWD
4	50	HGESS	IIIA	144	Peritoneum	12 y 6 mo	AWD
5	65	PEComa	IVB	N/A	Lung, lymph node	4 y 1 mo	DOD

AWD alive with disease, *DOD* died of disease, *HGESS* high-grade endometrial stromal sarcoma, *LGESS* low-grade endometrial stromal sarcoma, *mo* months, *N/A* not applicable (due to incomplete resection of disease at the time of initial diagnosis), *PEComa* perivascular epithelioid cell tumor, *y* years.

The uterine primary (Case1-Prim), lung metastasis (Case1-Met1), and vulvar recurrence (Case1-Recur1) were all diagnosed as LGESS with extensive sex cord differentiation. The uterine primary (Case1-Prim) was composed of epithelioid cells arranged as trabeculae (Fig. 2A), nests, and anastomosing cords (Fig. 2B) and demonstrating permeative myometrial and vascular invasion. The cells had enlarged oval to round nuclei with vesicular chromatin, 1–3 prominent nuclei, abundant eosinophilic cytoplasm, and a mitotic index of <1/10 HPF. Loose fibrous stroma, foamy macrophages (Fig. 2C), and a delicate capillary network were present. Similar morphologic features were seen in the lung and vulvar tumors (Case1-Met1/Recur1), the latter (Case1-Recur1) of which also demonstrated tubule formation (Fig. 2D), dense sclerosis surrounding tumor cells (Fig. 2E) and blood vessels, and an increased mitotic index of 10/10 HPF. A low-grade spindled component resembling conventional LGESS was also seen only in the vulvar recurrence (Case1-Recur1) and consisted of spindle cells with small oval to round nuclei, 1–2 indistinct nucleoli, and scant eosinophilic cytoplasm associated with perivascular whirling and a mitotic index of 6/10 HPF (Fig. 2F, G).

While CD10, ER, and PR combined scores were each >2 in the spindled component, CD10 and PR combined scores were both <1 in the epithelioid component (Figs. 2H and 3). Desmin combined scores were 2.7 and 1.8 in epithelioid and spindled components, respectively, while SMA was entirely negative. HMB45 combined score was <1 in both components (Fig. 2I), while A103 was entirely negative. Cathepsin K combined score was 3 in both components. pS6 combined score was >2 and <1 in the epithelioid and spindled components, respectively. BCOR was positive in only the epithelioid component, while cyclin D1 was positive in both.

A *JAZF1-SUZ12* fusion was detected in the vulvar recurrence (Case1-Recur1) (Table 2). Targeted massively parallel sequencing identified *TSC2* Y429* and L1575P mutations, in addition to a truncating mutation in *CCNE1* and missense mutations in *FAT1*, and *NF1* (Case1-Recur1) (Table 2).

With the detection of somatic *TSC2* mutations, the patient received mTORi with an investigational agent targeting mTOR and showed transient partial benefit until progressing after five months of therapy. She had an initial radiologic response and subsequent progression, therefore coming off protocol treatment after five months. Her initial response was notable for apparent necrosis of a left para-aortic node. After coming off protocol treatment, she received anastrozole and continued to progress until achieving stable disease while on megestrol acetate at last follow-up (Fig. 1).

Case 2

A 61-year-old patient presented with unresectable, diffusely metastatic disease with pathology confirmed on left supraclavicular lymph node (Case2-Met1) and vaginal (Case2-Met2) biopsies and received exemestane for 15 months (Table 1 and Fig. 1). She initially had partial response over four months. However, upon growth of the pelvic mass, she received leuprolide acetate and continued to have progression of disease on both lines of endocrine therapy. A biopsy of the left retroperitoneal tumor was performed (Case2-Met3).

Metastatic LGESS was diagnosed in the left supraclavicular lymph node, vaginal, and left retroperitoneal biopsies (Case2-Met1/Met2/Met3). The lesion in the lymph node and retroperitoneal biopsies (Case2-Met1/Met3) demonstrated conventional LGESS morphology and consisted of small spindle cells with oval to round nuclei, coarse chromatin, 1–2 indistinct nucleoli, and scant eosinophilic cytoplasm associated with perivascular whirling and a mitotic index of 2/10 HPF (Fig. 4A). The vaginal lesion (Case2-Met2), however, was composed of cords, trabeculae, and nests of epithelioid cells with enlarged oval to round nuclei, vesicular chromatin, 1–3 nucleoli, and abundant eosinophilic cytoplasm associated with a mitotic index

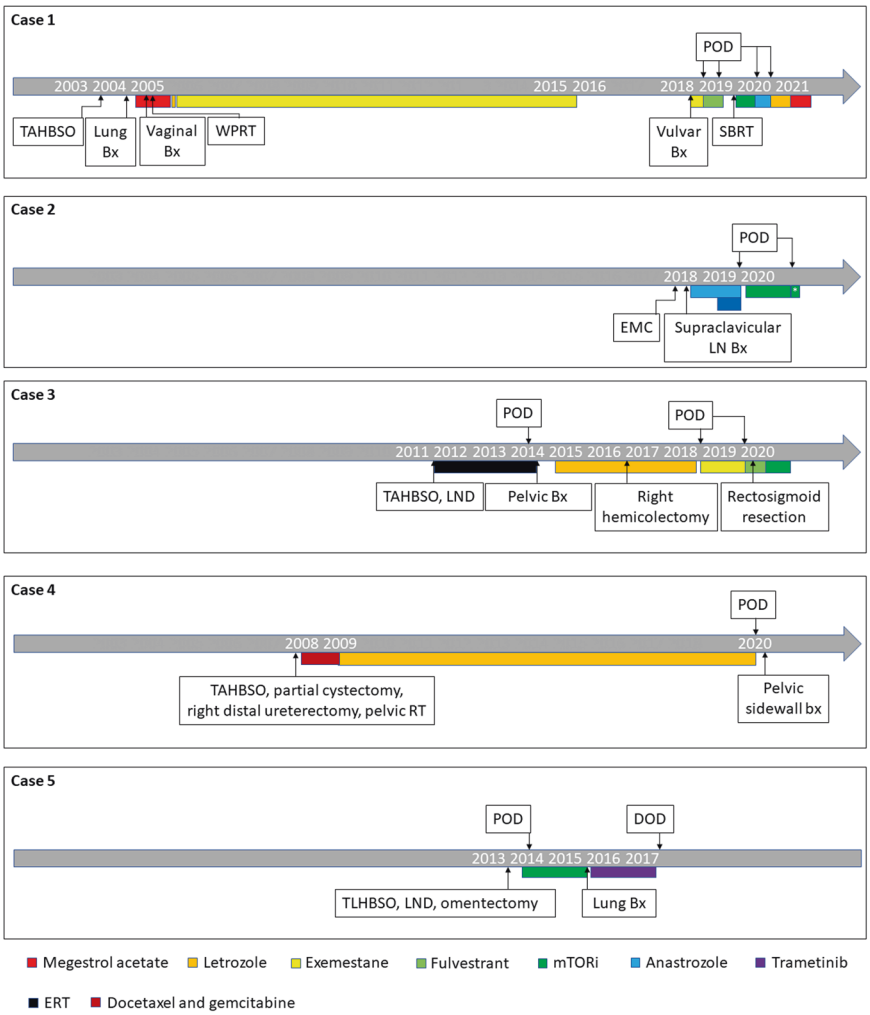

Fig. 1 Treatment timeline of the five patients with uterine sarcomas demonstrating LGESS, HGESS, and PEComa features included in this study. In cases 1–4, the patient was alive with disease at last follow-up indicated by a ray. In case 5, the patient died of disease, indicated by a line segment. An asterisk symbol indicates second-line mTORi. Bx biopsy, EMC endometrial curettage, ERT estrogen replacement therapy, LN lymph node, LND lymph node dissection, POD progression of disease, RT radiation therapy, SBRT single beam radiation therapy, TAHBSO total abdominal hysterectomy and bilateral salpingo-oophorectomy, TLHBSO total laparoscopic hysterectomy and bilateral salpingo oophorectomy, WPRT whole pelvic radiation therapy.

of <1/10 HPF and dense sclerosis surrounding tumor cells and blood vessels (Fig. 4B); no spindled component was seen.

CD10 (Fig. 4C), ER, and PR combined scores were each >2 in both spindled and epithelioid components (Fig. 3). Desmin staining was seen only in the spindled component with a combined score of 1.5. SMA was negative throughout. Cyclin D1 (Fig. 4D) was positive, while BCOR was negative in both components. Additional stains were evaluated only in the epithelioid component seen in the vaginal biopsy (Case2-Met2) that had sufficient material. HMB45 and A103 were negative. Cathepsin K and pS6 combined scores were >2.

A *JAZF1-SUZ12* fusion was detected in the lymph node metastasis (Case2-Met1) (Table 2). Massively parallel sequencing detected *TSC2* E787* and H1019Qfs*135 mutations along with a truncating *PTEN* mutation in the same tumor (Case2-Met1) (Table 2).

Noting the somatic *TSC2* mutations (Case2-Met1), the patient was treated with sirolimus, a commercial mTORi. She had an initial mixed radiologic response to sirolimus (4 mg/day) with necrosis in a bulky para-aortic mass. Her dose of sirolimus was decreased to 1 mg/day due to fevers, inflammation, and thrombosis of the left renal vein, adjacent to a necrotic (biopsy-proven) left para-aortic node. Subsequent scans showed radiologic improvement in all lesions. The sirolimus dose was incrementally increased to 4 mg/day; however, she developed progression after 10 months. She was subsequently treated with a second-line investigational mTORi (Fig. 1); treatment is ongoing at six months.

Case 3

A 55-year-old patient underwent laparoscopic hysterectomy, BSO, and lymph node dissection (LND) for an endometrial stromal tumor previously found on endometrial curettage (Case3-Prim) (Table 1 and Fig. 1). She had no residual tumor postoperatively and received estrogen replacement therapy (ERT) from her local provider. After three years, she developed vaginal, pelvic, and lower abdominal disease. ERT was discontinued, and letrozole was started. She had stable disease and underwent multi-site small-volume disease resection (Case3-Recur1). She had no evidence of disease for two years until a pelvic mass appeared. She received exemestane and underwent sigmoid resection (Case3-Recur2). After further radiologic progression, she received fulvestrant for two months.

The uterine primary (Case3-Prim) was diagnosed on endometrial curettage as an endometrial stromal tumor with LGESS and endometrial stromal nodule considered in the differential. The tumor demonstrated LGESS morphology and consisted of small

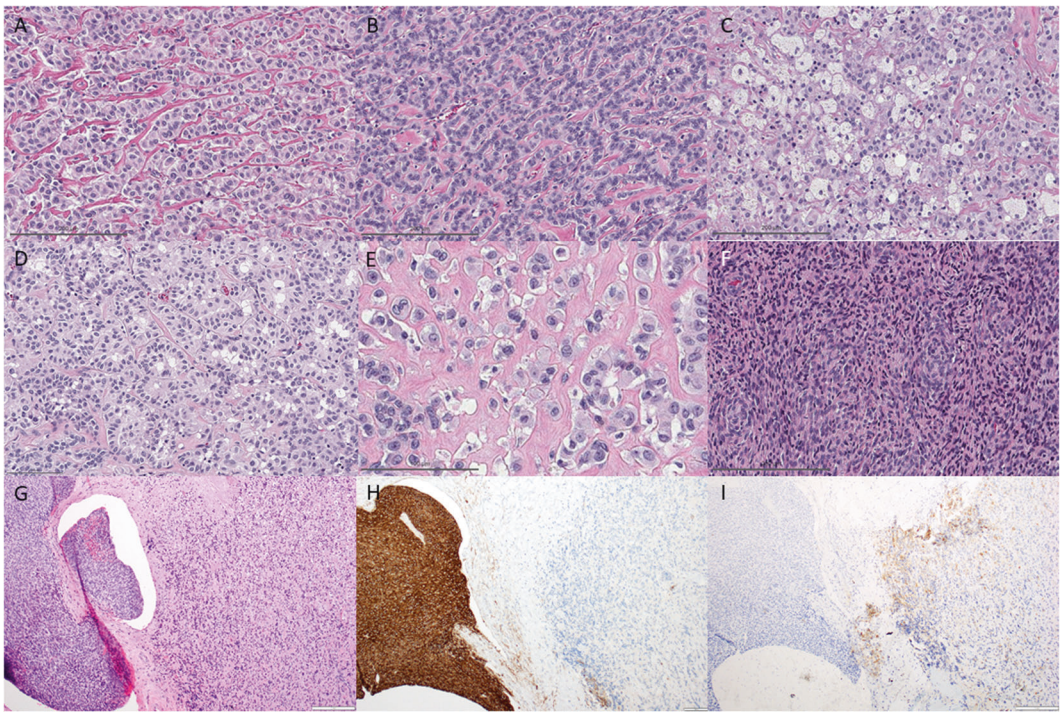

Fig. 2 Case 1. The epithelioid cells of the uterine primary (Case1-Prim) formed (**A**) trabeculae and (**B**) anastomosing cords associated with (**C**) foamy macrophages. Similar features were also seen in the lung metastasis (Case1-Met1) and vulvar recurrence (Case1-Recur1) which demonstrated epithelioid cells forming (**D**) tubules, (**E**) clusters, and single cells surrounded by sclerosis. (**F**, **G**) A low-grade spindled component resembling conventional low-grade endometrial stromal sarcoma was only seen in the vulvar recurrence (Case1-Recur1). (**H**, **I**) CD10 and HMB45 staining was seen in both spindled (left) and epithelioid (right) components.

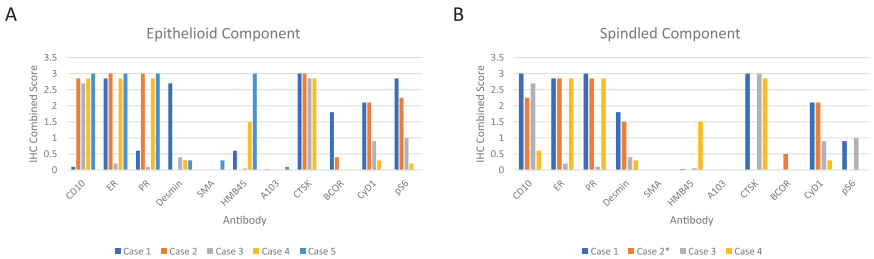

Fig. 3 Immunohistochemical (IHC) combined scores in the epithelioid and when present spindled components of TSC2-mutant uterine sarcomas. A Epithelioid component, **B** Spindled component. IHC combined scores were calculated by multiplying the percentage of positive tumor cells by the intensity of staining which was recorded as weak (1), moderate (2), and strong (3). Case 2 did not have sufficient material for SMA staining of the epithelioid and spindled components and for HMB45, A103, and cathepsin K staining of the spindled component. Case 5 did not have sufficient material for cathepsin K, BCOR, and cyclin D1 staining in the epithelioid cells; no spindled component was seen in the uterine primary or lung metastasis (Case5-Prim/Met1). A103 melan-A, CTSK cathepsin K, CyD1 cyclin D1, ER estrogen receptor, PR progesterone receptor, pS6 phospho-S6, SMA smooth muscle actin.

spindle cells with oval to round nuclei, coarse chromatin, small nuclei, and scant eosinophilic cytoplasm, associated with perivascular whirling and a mitotic index of <1/10 HPF. Smooth muscle differentiation was evident in the form of spindled cells with moderate amount of eosinophilic cytoplasm forming bundles and a starburst pattern of hyalinization. Both recurrences (Case3-Recur1/Recur2) were diagnosed as LGESS with variant epithelioid or sex cord features. The first recurrence (Case3-Recur1) consisted of only epithelioid cells arranged in anastomosing cords, trabeculae, single cells, and nests (Fig. 5A, B). The cells showed large, oval to round nuclei, vesicular chromatin, 1–2 prominent nucleoli, and moderate to abundant eosinophilic and vacuolated cytoplasm; mitotic index was <1/10 HPF. Multinucleated bizarre and Touton giant cells and dense sclerosis were present (Fig. 5A, B). The second recurrence (Case3-Recur2) consisted of both epithelioid and spindled components (Fig. 5C) morphologically similar to the primary and recurrent tumor (Case3-Prim/Recur1) and demonstrated foamy macrophages.

CD10, ER, PR, desmin, and HMB45 (Fig. 5D) combined scores were each >2, <1, <1, <1, and <1, respectively, in both epithelioid and spindled components (Fig. 3). BCOR, cyclin D1, SMA, and A103 were negative. Cathepsin K and pS6 combined scores were >2 and 1, respectively, in both components.

A *JAZF1-SUZ12* fusion was detected in the first recurrence (Case3-Recur1) (Table 2). Massively parallel sequencing detected *TSC2* C646* and W1194* in the second recurrence (Case3-Recur2) (Table 2). In addition to *NTRK1* amplification, missense mutations in *AR* and *IL7R* were detected (Case3-Recur2) (Table 2).

After detection of somatic *TSC2* mutations, the patient received investigational mTORi. She showed radiographic response of liver lesions (Fig. 5E, F) and stable peritoneal disease (Fig. 5G, H) after 14 months of treatment (Fig. 1).

Table 2. Mutation profile of uterine sarcomas.

Tumor sample	Morphology	Gene fusion	Mutation	Sequencing type
Case1-Recur1	Epithelioid and spindled	*JAZF1-SUZ12*	*CCNE1* R374* *FAT1* T3595I *NF1* C2453Y *TSC2* Y429* *TSC2* L1575P	MSK-Solid Fusion, MSK-IMPACT
Case2-Met1	Spindled	*JAZF1-SUZ12*	*PTEN* K260Nfs* *TSC2* 787* *TSC2* H1019Qfs*135	MSK-Solid Fusion, MSK-IMPACT
Case3-Recur1	Epithelioid	*JAZF1-SUZ12*		MSK-Solid Fusion
Case3-Recur2	Epithelioid and spindled		*NTRK1* amplification *AR* H41Q *IL7R* K395R *TSC2* C646* *TSC2* W1194*	MSK-IMPACT
Case4-Prim	Epithelioid and spindled	Failed		MSK-Solid Fusion
Case4-Recur2	Epithelioid	Negative	*TSC2* W358* *TSC2* S1482fs	MSK-Solid Fusion, Caris Next Generation Profiling
Case5-Prim	Epithelioid	*JAZF1-SUZ12*	*TSC2* exon 11 splicing variant[a]	MSK-Solid Fusion, MSK-IMPACT
Case5-Met1	Epithelioid		*TSC2* exon 11 splicing variant[a] *IKZF1* deletion	MSK-IMPACT

[a]Loss of heterozygosity.

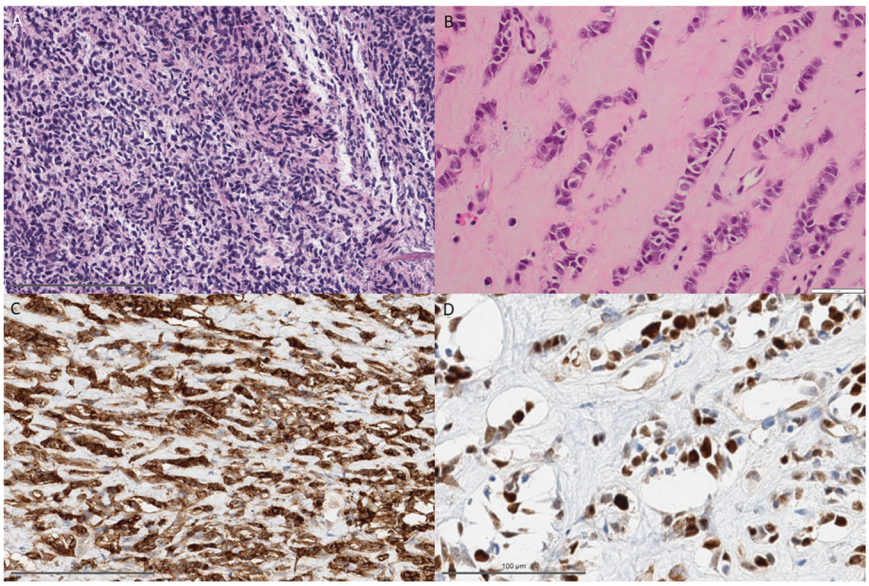

Fig. 4 Case 2. The lymph node and retroperitoneal biopsies (Case2- Met1/Met3) consisted of only a (**A**) spindled component resembling lowgrade endometrial stromal sarcoma. The vaginal biopsy (Case2-Met2) consisted of only (**B**) epithelioid cells forming trabeculae in a background of dense sclerosis. The epithelioid cells expressed (**C**) CD10 and (**D**) cyclin D1.

Case 4

A 50-year-old patient underwent primary TAHBSO (Case4-Prim), partial cystectomy, and right distal ureterectomy and then received six cycles of docetaxel and gemcitabine and pelvic EBRT postoperatively, followed by letrozole (Table 1 and Fig. 1). Eleven years later, while on letrozole, she developed right pelvic sidewall (Case4-Recur1) and bladder soft tissue (Case 4-Recur2) recurrences that were surgically resected.

The uterine primary (Case4-Prim) consisted of epithelioid and spindled cells permeating the myometrium (Fig. 6A–C). Most of the tumor demonstrated conventional LGESS morphology in the form of spindle cells with oval to round nuclei, coarse chromatin, indistinct nucleoli, and scant eosinophilic cytoplasm associated with perivascular whirling and a mitotic index of <1/10 HPF (Fig. 6B, C). There were, however, numerous foci of epithelioid cells with enlarged nuclei, prominent nucleoli, and abundant eosinophilic and vacuolated cytoplasm, forming cords, trabeculae, nests, and pseudopapillae, embedded in a background of sclerosis and associated with a mitotic index of 4/10 HPF (Fig. 6B, C). Foamy macrophages and lymphovascular invasion were present. The tumor was diagnosed as HGESS based on the cytologic features of the epithelioid foci surpassing those acceptable for LGESS (Fig. 6B, C). Both recurrences (Case4-Recur1/Recur2) demonstrated only epithelioid morphology similar to that seen in the uterine primary (Case4-Prim).

ER and PR combined scores were each >2 in both epithelioid and spindled components, while CD10 combined score was >2

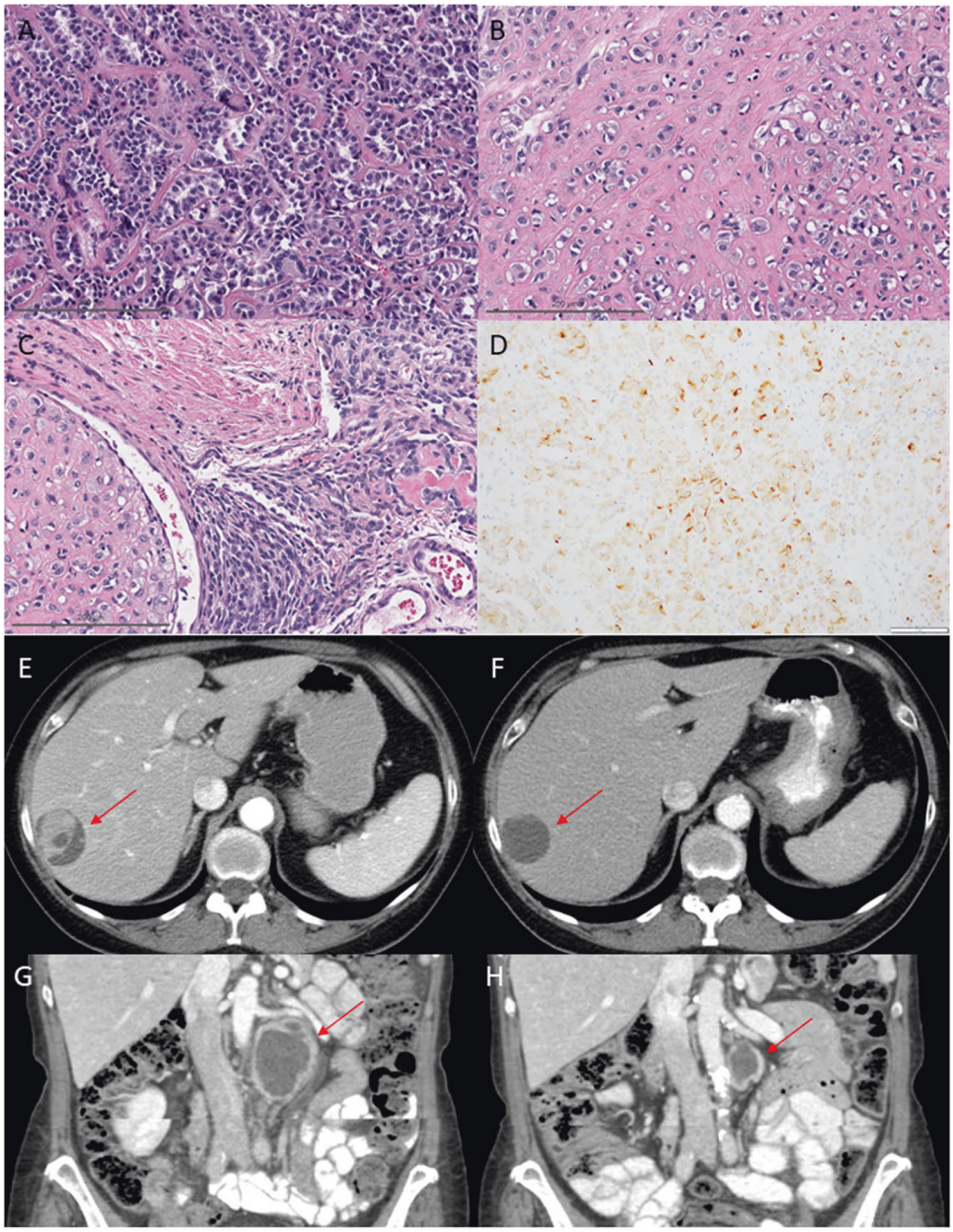

Fig. 5 Case 3. The first recurrence (Case3-Recur1) consisted of only epithelioid cells arranged in (**A**) anastomosing cords and trabeculae associated with Touton giant cells as well as (**B**) single cells and nests. The second recurrence (Case3-Recur2) consisted of (**C**) both epithelioid (left) and spindled right) components, the latter also demonstrating hyalinization typically seen in low-grade endometrial stromal sarcoma. (**D**) Desmin staining is seen in the epithelioid cells. Axial CT images from (**E**) at baseline, 17 days prior to starting mTORi showing parenchymal hepatic metastasis (red arrow) and (**F**) follow-up imaging 40 days after starting mTORi showing necrosis and reduction (red arrow). Coronal CT images from (**G**) at baseline, 6 days prior to starting mTORi showing left paraaortic nodal metastasis (red arrow) and (**H**) follow-up imaging 37 days after starting mTORi showing reduction in size of necrotic tumor (red arrow).

and <1 in the epithelioid and spindled components (Figs. 3 and 6D), respectively. Desmin staining was limited, while SMA was negative in both components. HMB45 and cathepsin K combined scores were 1.5 and >2, respectively, in both components (Figs. 6E, F). pS6 combined score was <1 in the epithelioid component only. BCOR (Fig. 6G), cyclin D1, and A103 were negative.

Targeted RNA NGS of the uterine primary (Case4-Prim) failed but was successful in the second recurrence (Case4-Recur2) in which no fusions were detected (Table 2). FISH did not show *JAZF1* rearrangement (Case4-Recur2). Massively parallel sequencing detected *TSC2* W358* and S1482fs in the second recurrence (Case4-Recur2) (Table 2).

The patient was not treated with mTORi and discontinued care at our institution.

Case 5

A 65-year-old patient underwent laparoscopic hysterectomy (Case5-Prim), BSO, pelvic, and para-aortic LND, and omentectomy at an outside institution, complicated by fragmentation of the uterus with manipulation upon specimen removal (Table 1 and Fig. 1). She was initially diagnosed with HGESS at the outside hospital that was revised to malignant PEComa based on subsequent review of pathologic and molecular genetic findings, as reported previously[24]. She was monitored expectantly until six

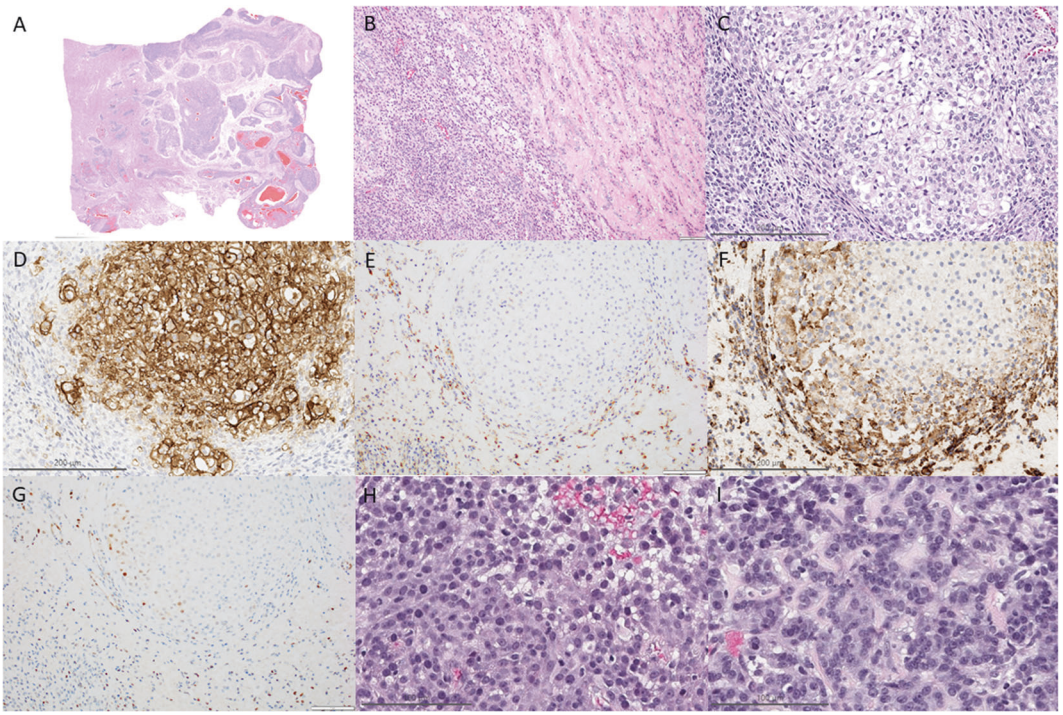

Fig. 6 Cases 4 and 5. The primary tumor (Case4-Prim) in case 4 demonstrated (**A**) permeative myometrial invasion and consisted of (**B**, **C**) epithelioid components forming nodules (right) surrounded by low-grade spindled cells (left). (**D**) CD10 staining was predominately seen in the epithelioid component (right), while (**E**) HMB45 staining was seen in the spindled component (left). (**F**) Cathepsin K was expressed in both epithelioid (right) and spindled (left) foci. (**G**) Both components showed limited cyclin D1 staining which was considered a negative pattern. The lung metastasis of case 5 (Case5-Met1) showed only epithelioid cells forming (**H**) sheets and (**I**) cords.

months postoperatively when imaging revealed retroperitoneal and left pelvic lymphadenopathy and progression of bilateral lung nodules (Case5-Met1).

The uterine primary (Case5-Prim) consisted of only epithelioid cells arranged in nests and trabeculae associated with sclerotic collagenous septa, permeative myometrial invasion, lymphovascular invasion, and a mitotic index of 14/10 HPF. The lung metastasis (Case5-Met1) showed similar morphology (Fig. 6H, I). No spindled component was seen in primary or metastatic tumor (Case5-Prim/Met1).

The uterine primary (Case5-Prim) showed CD10, ER, and PR combined scores of 3 each (Fig. 3). HMB45 and A103 stains were available for review and demonstrated combined scores of 3 and <1, respectively. Based on the HMB45 staining pattern and epithelioid morphology, a diagnosis of PEComa was rendered.

JAZF1-SUZ12 fusion and a *TSC2* exon 11 splicing variant with broad copy number loss of chromosome arm 16q suggesting loss of heterozygosity were detected in the primary tumor (Case5-Prim) (Table 2). In addition to the *TSC2* exon 11 splicing variant, a *IKZF1* deletion was also detected in lung metastasis (Case5-Met1) (Table 2).

The patient was subsequently treated with an mTORi with best response stable disease, then developed slow progression in pelvic and lung lesions. Total duration of treatment was 17 months. She died of disease (Fig. 1).

Summary of histologic, immunophenotypic, and molecular findings

In the cases for which hysterectomy slides were available for review, the tumor demonstrated permeative myometrial and vascular invasion (Fig. 6A). In all five cases, an epithelioid component was present and consisted of nodules with sclerotic stroma (Figs. 2 and 4–6). Within nodules, cells formed sheets, cords, nests, and trabeculae. Retiform growth, pseudopapillae, single cells, and tubules were occasionally present. Median mitotic index was 4 (range, 1–14)/10 HPF. A spindled component resembling LGESS was present in four tumors, adjacent to epithelioid foci and forming sheets of bland cells with coarse chromatin, indistinct nucleoli, and scant eosinophilic cytoplasm and perivascular whirling. Mitotic index was <1 per 10 HPF (Figs. 2 and 4–6).

Both spindled (when present) and epithelioid components in all cases demonstrated at least focal CD10, ER, and PR expression (Fig. 3). Desmin was variable in extent and intensity in both components, while SMA was consistently negative. HMB45 and A103 expression were also variable in extent and intensity. Cathepsin K combined score was >2 in both components of all cases. pS6 expression with variable extent was seen in the epithelioid component.

Targeted DNA NGS revealed pathogenic somatic *TSC2* inactivating mutations in all cases (Table 2). Four recurrent tumors (Cases 1–4) harbored two independent *TSC2* mutations, likely representing biallelic inactivation. The remaining case (Case 5) demonstrated a *TSC2* exon 11 splicing variant with loss of heterozygosity in the primary tumor. Additional mutations were found in four tumors (Cases 1–3 and 5), but none were recurrent. Targeted RNA NGS revealed an in-frame fusion between *JAZF1* exon 3 and *SUZ12* exon 2 in four tumors (Table 2). In the remaining case (Case 4), no gene fusions were detected by targeted RNA NGS, and no *JAZF1* rearrangement was found by FISH.

Methylation profiling of uterine sarcomas

To assess whether epigenetic profiles of the *TSC2*-mutant tumors were related to LGESS and/or HGESS, DNA methylation profiling was performed on 4 *TSC2*-mutant uterine sarcomas (Cases 1–4) with available material, 10 LGESS, and 12 HGESS. When DNA methylation profiles were analyzed using a previously published sarcoma classifier[21], only one *TSC2*-mutant, fusion-negative tumor (Case 4) classified as LGESS methylation class family with high confidence (calibrated score = 0.91) by the classifier. The remaining three cases (Cases 1–3), all harboring *JAZF1-SUZ12* fusion, did

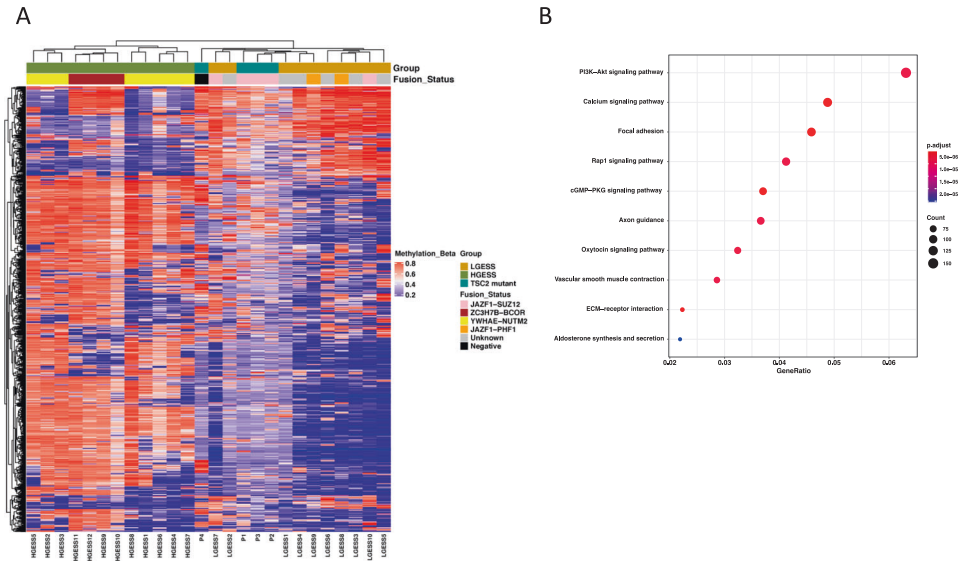

Fig. 7 Methylation profiling of TSC2-mutant uterine sarcomas. A Unsupervised hierarchical clustering analysis of TSC2-mutant uterine sarcomas, low-grade endometrial stromal sarcoma (LGESS), and highgrade endometrial stromal sarcoma (HGESS) based on methylated probes (blue indicates hypomethylation, and red indicates hypermethylation). HGESS formed a single cluster (left), while LGESS and TSC2 mutant uterine sarcomas formed a separate cluster (right). **B** KEGG pathway analysis demonstrates several pathways enriched in the top differentially methylated genes/probes. Dot plots represent the ratio of genes (x-axis) involved in each signaling pathway (y-axis). The size of the dots shows gene counts, and the color denotes significance level.

not match with any known methylation class family by the classifier, suggesting that *TSC2* mutation alters the DNA methylation signature affecting the ability of the machine learning algorithm to classify the tumors. This is likely because *TSC2*-mutant LGESS were not represented in the training cohort for the classifier development. However, when we performed independent unsupervised clustering analysis, DNA methylation profiles showed two distinct clusters (Fig. 7A). All HGESS harboring *ZC3H7B-BCOR* and *YWHAE-NUTM2A/B* fusions formed one cluster that was further divided into two subgroups: (1) *YWHAE* fusion-positive tumors only ($n = 5$) and (2) tumors harboring *YWHAE* ($n = 3$) or *BCOR* ($n = 4$) fusion. All LGESS formed a separate major cluster, which also included all *TSC2*-mutant uterine sarcomas. This cluster was divided into three subgroups: (1) LGESS harboring *JAZF1-SUZ12* ($n = 1$) or *JAZF1-PHF1* ($n = 1$) fusion or having unknown fusion status ($n = 3$), (2) *TSC2*-mutant uterine sarcoma with negative fusion status, and (3) all remaining *TSC2*-mutant uterine sarcomas with *JAZF1-SUZ12* fusion and all remaining LGESS harboring *JAZF1-SUZ12* ($n = 4$) or *JAZF1-PHF1* ($n = 1$) fusion or having unknown fusion status ($n = 1$). However, the small size of these subclusters precludes any assessment regarding their biological differences. KEGG pathway analysis of the top 10,000 most variably methylation genes/probes in the cohort demonstrated enrichment in pathways involving PI3K-AKT, calcium, and Rap1 signaling, among others (Fig. 7B).

DISCUSSION

In this study, we characterized the morphologic, immunohistochemical, genomic, and methylation profiles of uterine sarcomas demonstrating features of LGESS, HGESS, and PEComa. Through targeted NGS, we identified *TSC2* mutations and *JAZF1-SUZ12* fusions in 100% and 80% of cases, respectively. All tumors were epithelioid and often associated with a spindled component resembling LGESS, with both regions expressing CD10, ER, and PR; variable myomelanocytic differentiation; and pS6 staining. By methylation, all tumors clustered with LGESS, suggesting epigenetic similarity to LGESS. Functional genomic pathway analysis demonstrated upregulation of PIK3-AKT and Rap1 signaling. Lesions appeared responsive to hormone suppression. Patients treated with mTORi for progressive disease achieved clinical benefits.

These tumors share clinicopathologic, genetic, and epigenetic overlap with LGESS. They often demonstrate permeative myoinvasion; low-grade spindle foci; CD10, ER, and PR expression; and *JAZF1-SUZ12* fusion[25–32]. While only one tumor was classified as LGESS by methylation, all tumors shared largely similar epigenetic signatures with LGESS. Patients also appear to benefit from hormone blockade treatment. *SUZ12* encodes a component of the polycomb repressive complex (PRC) 2, a major class of histone methylation complexes that are involved in transcriptional repression[33]. The *JAZF1-SUZ12* fusion product may disrupt PRC2 complexes and impair chromatin repression[34,35].

While the most common LGESS-associated fusion was detected in four cases, no gene rearrangements were found by targeted RNA NGS of Case 4. Despite the absence of a detectable fusion, however, Case 4 was the only tumor that matched to the LGESS methylation class family. Given the frequency and diversity of gene fusions among endometrial stromal tumors, this tumor likely harbors a rare gene rearrangement that is currently not targeted by the MSK-Solid Fusion Assay.

Epithelioid morphology, expression of melanocytic markers, and presence of *TSC2* mutations suggest PEComa-like differentiation. Among LGESS, epithelioid change is rare[36–38] and HMB45 staining, variable[39,40]. Mutations involving *TSC2* detected in our tumors are also found in PEComas and have not been previously detected in LGESS[41]. *TSC2* encodes tuberin, which together with hamartin encoded by *TSC1* helps control cell growth and size[42]. The detection of two *TSC2* mutations in each tumor suggests biallelic inactivation of this tumor suppressor gene. As expected, tumors demonstrated strong pS6 staining, suggesting hyperactive mTORC1 signaling. While it is difficult to determine whether *TSC2* mutations are acquired or de novo in a small cohort with limited material available for sequencing, *TSC2* mutations were detected in the primary uterine tumor of one patient suggesting de novo genetic alterations. Observed partial responses to mTORi suggest that mTOR-targeted therapy may be beneficial in patients with *TSC2*-mutant uterine sarcomas who develop progressive disease on hormone blockade[43,44].

This study has several important limitations. Uterine sarcomas that harbor *TSC2* mutations with or without concurrent LGESS-associated gene fusions are rare. Despite the small sample size, however, our cohort consists of a histologically, genetically, and epigenetically homogeneous group of tumors. While it is notable that most patients in our cohort initially presented with advanced stage disease, clinical outcome data remain limited owing to the rarity of these lesions. We were also unable to identify gene fusions in one case by targeted RNA NGS. While the presence of *TSC2* mutations in the uterine primary of one case suggests de novo alterations, we were unable to confirm this observation by sequencing primary tumors of the remaining cases due to the limited material available from the cases analyzed. Further studies of *TSC2*-mutant uterine sarcomas are warranted, including whole transcriptome sequencing of fusion-negative tumors as well as mutation profiling of matched uterine primaries and recurrences. Long-term clinical follow-up of these rare indolent cancers is also necessary.

We recognize that access to the sequencing modalities used in this study may be limited in most pathology practices and may not be needed for diagnostic or therapeutic purposes in the majority of LGESS patients. Given the implications for targeted therapy, however, *TSC2* mutational profiling may be helpful in the setting of any uterine mesenchymal tumor demonstrating epithelioid histology, nuclear uniformity, and myomelanocytic differentiation, particularly when the following entities are considered in the differential diagnosis: (1) LGESS or HGESS with epithelioid change, (2) LGESS or HGESS with sex cord differentiation, and (3) PEComa. Mutational profiling is also recommended in the setting of LGESS exhibiting unusual clinical behavior.

Lastly, DNA methylation profiling has shown promise for diagnosis and classification of various cancers including brain tumors and sarcomas[21,45]. Our data show that secondary mutations, not represented in the reference cohorts used in the development of the classifier, can affect the performance, and higher number of samples with concurrent mutational and fusion profiles will be necessary.

In summary, we describe a histologically distinctive group of uterine sarcomas that are characterized by *TSC2* mutations, hyperactive mTORC1 signalizing, and frequent *JAZF1-SUZ12* fusions. Patients with these tumors demonstrated responses to endocrine therapy and to mTORi. We favor using the term "LGESS, *TSC2*-mutant" given a disease-defining fusion, indolent clinical behavior, and response to both endocrine and mTOR pathway targeted therapy.

DATA AVAILABILITY

The datasets used and/or analyzed during the current study are available from the corresponding author on reasonable request.

REFERENCES

1. Thway, K. & Fisher, C. PEComa: morphology and genetics of a complex tumor family. *Ann. Diagn. Pathol.* **19**, 359–368 (2015).
2. Hornick, J. L. & Fletcher, C. D. PEComa: what do we know so far? *Histopathology* **48**, 75–82 (2006).
3. Giannikou, K. et al. Whole exome sequencing identifies TSC1/TSC2 biallelic loss as the primary and sufficient driver event for renal angiomyolipoma development. *PLoS Genet* **12**, e1006242 (2016).
4. Bennett, J. A. et al. Uterine PEComas: a morphologic, immunohistochemical, and molecular analysis of 32 tumors. *Am. J. Surg. Pathol.* **42**, 1370–1383 (2018).
5. Agaram, N. P. et al. Dichotomy of genetic abnormalities in PEComas with therapeutic implications. *Am. J. Surg. Pathol.* **39**, 813–825 (2015).
6. Schoolmeester, J. K. et al. TFE3 translocation-associated perivascular epithelioid cell neoplasm (PEComa) of the gynecologic tract: morphology, immunophenotype, differential diagnosis. *Am. J. Surg. Pathol.* **39**, 394–404 (2015).
7. Conlon, N., Soslow, R. A. & Murali, R. Perivascular epithelioid tumours (PEComas) of the gynaecological tract. *J. Clin. Pathol.* **68**, 418–426 (2015).
8. Schoolmeester, J. K. et al. Perivascular epithelioid cell neoplasm (PEComa) of the gynecologic tract: clinicopathologic and immunohistochemical characterization of 16 cases. *Am. J. Surg. Pathol.* **38**, 176–188 (2014).
9. Bleeker, J. S., Quevedo, J. F. & Folpe, A. L. "Malignant" perivascular epithelioid cell neoplasm: risk stratification and treatment strategies. *Sarcoma* **2012**, 541626 (2012).
10. Folpe, A. L. et al. Perivascular epithelioid cell neoplasms of soft tissue and gynecologic origin: a clinicopathologic study of 26 cases and review of the literature. *Am. J. Surg. Pathol.* **29**, 1558–1575 (2005).
11. Starbuck, K. D., Drake, R. D., Budd, G. T. & Rose, P. G. Treatment of advanced malignant uterine perivascular epithelioid cell tumor with mTOR inhibitors: single-institution experience and review of the literature. *Anticancer Res.* **36**, 6161–6164 (2016).
12. McCormack, F. X. et al. Efficacy and safety of sirolimus in lymphangioleiomyomatosis. *N. Engl. J. Med.* **364**, 1595–1606 (2011).
13. Wagner, A. J. et al. Clinical activity of mTOR inhibition with sirolimus in malignant perivascular epithelioid cell tumors: targeting the pathogenic activation of mTORC1 in tumors. *J. Clin. Oncol.* **28**, 835–840 (2010).
14. Vang, R. & Kempson, R. L. Perivascular epithelioid cell tumor ('PEComa') of the uterus: a subset of HMB-45-positive epithelioid mesenchymal neoplasms with an uncertain relationship to pure smooth muscle tumors. *Am. J. Surg. Pathol.* **26**, 1–13 (2002).
15. Hornick, J. L. & Fletcher, C. D. Sclerosing PEComa: clinicopathologic analysis of a distinctive variant with a predilection for the retroperitoneum. *Am. J. Surg. Pathol.* **32**, 493–501 (2008).
16. Zhu, G. et al. Diagnosis of known sarcoma fusions and novel fusion partners by targeted RNA sequencing with identification of a recurrent ACTB-FOSB fusion in pseudomyogenic hemangioendothelioma. *Mod. Pathol.* **32**, 609–620 (2019).
17. Zehir, A. et al. Mutational landscape of metastatic cancer revealed from prospective clinical sequencing of 10,000 patients. *Nat. Med.* **23**, 703–713 (2017).
18. Cheng, D. T. et al. Memorial Sloan Kettering-Integrated Mutation Profiling of Actionable Cancer Targets (MSK-IMPACT): a hybridization capture-based next-generation sequencing clinical assay for solid tumor molecular oncology. *J. Mol. Diagn.* **17**, 251–264 (2015).
19. Chakravarty, D., et al. OncoKB: a precision oncology knowledge base. *JCO Precis. Oncol.* **2017**, PO.17.00011 (2017).
20. Serrano, J. & Snuderl, M. Whole genome DNA methylation analysis of human glioblastoma using Illumina BeadArrays. *Methods Mol. Biol.* **1741**, 31–51 (2018).
21. Koelsche, C. et al. Sarcoma classification by DNA methylation profiling. *Nat. Commun.* **12**, 498 (2021).
22. Aryee, M. J. et al. Minfi: a flexible and comprehensive bioconductor package for the analysis of Infinium DNA methylation microarrays. *Bioinformatics* **30**, 1363–1369 (2014).
23. Yu, G., Wang, L. G., Han, Y. & He, Q. Y. clusterProfiler: an R package for comparing biological themes among gene clusters. *OMICS* **16**, 284–287 (2012).
24. Selenica, P. et al. Genomic profiling aids classification of diagnostically challenging uterine mesenchymal tumors with myomelanocytic differentiation. *Am. J. Surg. Pathol.* **45**, 77–92 (2021).
25. Hodge, J. C., Bedroske, P. P., Pearce, K. E. & Sukov, W. R. Molecular cytogenetic analysis of JAZF1, PHF1, and YWHAE in endometrial stromal tumors: discovery of genetic complexity by fluorescence in situ hybridization. *J. Mol. Diagn.* **18**, 516–526 (2016).
26. Jakate, K. et al. Endometrial sarcomas: an immunohistochemical and JAZF1 rearrangement study in low-grade and undifferentiated tumors. *Mod. Pathol.* **26**, 95–105 (2013).
27. Chiang, S. et al. Frequency of known gene rearrangements in endometrial stromal tumors. *Am. J. Surg. Pathol.* **35**, 1364–1372 (2011).
28. Kurihara, S. et al. Endometrial stromal sarcomas and related high-grade sarcomas: immunohistochemical and molecular genetic study of 31 cases. *Am. J. Surg. Pathol.* **32**, 1228–1238 (2008).
29. Nucci, M. R., Harburger, D., Koontz, J., Dal Cin, P. & Sklar, J. Molecular analysis of the JAZF1-JJAZ1 gene fusion by RT-PCR and fluorescence in situ hybridization in endometrial stromal neoplasms. *Am. J. Surg. Pathol.* **31**, 65–70 (2007).
30. Hrzenjak, A. et al. JAZF1/JJAZ1 gene fusion in endometrial stromal sarcomas: molecular analysis by reverse transcriptase-polymerase chain reaction optimized for paraffin-embedded tissue. *J. Mol. Diagn.* **7**, 388–395 (2005).
31. Huang, H. Y., Ladanyi, M. & Soslow, R. A. Molecular detection of JAZF1-JJAZ1 gene fusion in endometrial stromal neoplasms with classic and variant histology: evidence for genetic heterogeneity. *Am. J. Surg. Pathol.* **28**, 224–232 (2004).
32. Koontz, J. I. et al. Frequent fusion of the JAZF1 and JJAZ1 genes in endometrial stromal tumors. *Proc. Natl Acad. Sci. USA.* **98**, 6348–6353 (2001).
33. Healy, E. et al. PRC2.1 and PRC2.2 synergize to coordinate H3K27 trimethylation. *Mol. Cell* **76**, 437–452 e436 (2019).
34. Ma, X. et al. The JAZF1-SUZ12 fusion protein disrupts PRC2 complexes and impairs chromatin repression during human endometrial stromal tumorogenesis. *Oncotarget* **8**, 4062–4078 (2017).
35. Li, H. et al. Effects of rearrangement and allelic exclusion of JJAZ1/SUZ12 on cell proliferation and survival. *Proc. Natl Acad. Sci. USA.* **104**, 20001–20006 (2007).

36. Baker, P. M., Moch, H. & Oliva, E. Unusual morphologic features of endometrial stromal tumors: a report of 2 cases. *Am. J. Surg. Pathol.* **29**, 1394–1398 (2005).
37. Goh, S. G., Chuah, K. L., Chew, S. H. & Tan, P. H. Uterine epithelioid endometrial stromal sarcoma presenting as a "cervical polyp". *Ann. Diagn. Pathol.* **9**, 101–105 (2005).
38. Oliva, E., Clement, P. B. & Young, R. H. Epithelioid endometrial and endometrioid stromal tumors: a report of four cases emphasizing their distinction from epithelioid smooth muscle tumors and other oxyphilic uterine and extrauterine tumors. *Int. J. Gynecol. Pathol.* **21**, 48–55 (2002).
39. Albores-Saavedra, J. et al. Endometrial stromal sarcomas: immunoprofile with emphasis on HMB45 reactivity. *Am. J. Clin. Pathol.* **141**, 850–855 (2014).
40. Abeler, V. M. & Nenodovic, M. Diagnostic immunohistochemistry in uterine sarcomas: a study of 397 cases. *Int. J. Gynecol. Pathol.* **30**, 236–243 (2011).
41. Hensley, M. L. et al. Genomic landscape of uterine sarcomas defined through prospective clinical sequencing. *Clin. Cancer Res.* **26**, 3881–3888 (2020).
42. Laplante, M. & Sabatini, D. M. mTOR signaling. *Cold Spring Harb. Perspect. Biol.* **4**, a011593 (2012).
43. Martin-Liberal, J., Benson, C., Messiou, C., Fisher, C. & Judson, I. Reversion of hormone treatment resistance with the addition of an mTOR inhibitor in endometrial stromal sarcoma. *Case Rep. Med.* **2014**, 612496 (2014).
44. Quan, P. et al. Effects of targeting endometrial stromal sarcoma cells via histone deacetylase and PI3K/AKT/mTOR signaling. *Anticancer Res.* **34**, 2883–2897 (2014).
45. Capper, D. et al. DNA methylation-based classification of central nervous system tumours. *Nature* **555**, 469–474 (2018).

AUTHOR CONTRIBUTIONS

Conception and design: S. Chiang, M.S., J.A.K. Financial support: N.R. A.-R. Provision of study material or patients: S. Chiang, L.H.E., K.J.P., R.M., R.A.S., C.-H.L., C.J.R.S., E.O., M.L.H., S.Cohen, C.A., M.A.D., J.A.K. Collection and assembly of data: S. Chiang, L.H.E., K.J.P., R.M., R.A.S., M.L.H., S. Cohen, C.A., M.A.D., J.A.K. Data analysis and interpretation: V.V., J.S., A.M.-B., A.A.J., A.D.C.P., E.M.d.S., B.W., R.B., M.L., M.S., S. Chiang, J.A.K. Manuscript writing: S. Chiang, J.A.K. Final approval of manuscript: all authors.

FUNDING

The study was supported in part by the MSK Cancer Center Support Grant P30 CA008748. B. W. was funded in part by Cycle for Survival, Breast Cancer Research Foundation and Stand Up to Cancer grants.

COMPETING INTERESTS

N.R. A.-R. reports institutional grants from Stryker/Novadaq, Olympus, and GRAIL, outside the submitted work. M.L.H. reports spouse employment by Sanofi, advisory board consulting for Tesaro, Glaxo Smith Kline. S. Chiang reports consulting for AstraZeneca. The remaining authors have no conflicts of interest to declare.

ETHICAL APPROVAL

Institutional Review Board approval was obtained at Memorial Sloan Kettering Cancer Center (MSKCC).

ADDITIONAL INFORMATION

Correspondence and requests for materials should be addressed to Sarah Chiang or Jason A. Konner.